Comput. Methods Appl. Mech. Engrg. 191 (2002) 5515–5536

Computer methods in applied mechanics and engineering

www.elsevier.com/locate/cma

A low order Galerkin finite element method for the Navier–Stokes equations of steady incompressible flow: a stabilization issue and iterative methods

Maxim A. Olshanskii

Department of Mechanics and Mathematics, Moscow State University, Moscow 119899, Russia

Received 25 May 2001; received in revised form 10 June 2002

Abstract

A Galerkin finite element method is considered to approximate the incompressible Navier–Stokes equations together with iterative methods to solve a resulting system of algebraic equations. This system couples velocity and pressure unknowns, thus requiring a special technique for handling. We consider the Navier–Stokes equations in velocity—kinematic pressure variables as well as in velocity—Bernoulli pressure variables. The latter leads to the rotation form of nonlinear terms. This form of the equations plays an important role in our studies. A consistent stabilization method is considered from a new view point. Theory and numerical results in the paper address both the accuracy of the discrete solutions and the effectiveness of solvers and a mutual interplay between these issues when particular stabilization techniques are applied.

Keywords: Navier–Stokes equations; Finite elements; Stabilized method; Oseen problem; Iterative methods

1. Introduction

In this paper we consider the steady incompressible Navier–Stokes equations (1). Typically to solve a computational fluid dynamic problem a researcher is free to build a method in many ways by choosing different discretization techniques, solvers for resulting discrete system, and setting a lot of parameters to some particular values. A lot of tools are available to treat the problem (1) numerically. For example one can choose a method from a family of finite differences, finite elements or finite volumes. Further a pseudotime stepping or another iterative solver for the nonlinear problem can be applied to find time-independent solutions. One can try to reformulate the original continuous problem and doing that to obtain discrete systems with different properties. These and many other particular ingredients can be put together in many ways and this may crucially influence the quality of a final solution obtained as well as the total

E-mail address: ay@olshan.msk.ru (M.A. Olshanskii).

0045-7825/02/$ - see front matter © 2002 Published by Elsevier Science B.V.
PII: S0045-7825(02)00513-3

CPU time of computations. Although the "best" method, if it exists, seems to be problem dependent, a reasonable objective is a method, which is able to solve a possibly widest class of problems efficiently, i.e. with acceptable guaranteed accuracy and CPU time. Recently a considerable effort has been made to *compare* the performance of various tools for simulating flow problems (see, e.g., [14,27,28,36,42], and monograph [44]) and to derive optimal schemes. Nevertheless a demand for predictable, robust, and efficient solvers/methods still exists. A good candidate for such a method is a finite element method for the "true" mixed formulation of the Navier–Stokes equations, since applied properly it has good stability properties and gives the possibility of the *rigorous* error control (e.g., [41]). However, the method is efficient only if the resulting discrete systems, having a quite complicated structure, can be solved efficiently.

The present paper is concerned with both the accuracy of the FE method *and* the numerical performance of linear algebra tools applied here to solve discrete systems. We are in no way exhaustive in these topics and concentrate further on techniques and results which are new, mentioning briefly those which are standard. The total machinery applied to treat the problem consists of the following basic tools:

(a) A low order FE method (P1isoP2/P0 in experiments). Two types of consistent stabilization are additionally considered. One is the SUPG method, another one amounts in adding particular term derived from the continuity equation to the momentum one.
(b) The fixed point or implicit backward Euler (BE) method to find a steady solution to a nonlinear problem.
(c) A block-triangular preconditioning combined with the BiCGstab iterations to solve the linearized Navier–Stokes problem (of Oseen type).
(d) Geometric multi-grid methods to solve or to approximate subproblems for velocity and pressure, which appear in item (c).

Details can be found in the next sections.

Non of the items (a)–(d) is absolutely new. Although the particular way of combining them is something we do not find in the literature, similar "configurations" can be found in [44]. However, we emphasize in the paper several ingredients which are new or not well studied, but were found to improve the overall performance of the method. Referring to the remainder of the paper for details, we outline them briefly:

(a) The rotation form of the Navier–Stokes equations (2) is a starting point for FE approximation in some experiments. It also appears to be useful for theoretical analysis of a solver performance. Where appropriate we will compare the performance of the rotation form with more commonly used convection form (1).
(b) A particular stabilization method is studied numerically and understood from the theoretical point of view: An additional term, $\gamma\nabla\mathrm{div}\,\mathbf{u}$, resulting from the continuity equation is added to the momentum one. Early this term has appeared in residual-based stabilization methods (e.g., [17,33]), but its role remained not very clear. We will see that the adding of this term intends to reduce the loss of accuracy, which the discrete solution suffers for small viscosity values due to the presence of the first-order pressure term (see Section 2.1). In the theory this effect does not depend on convection, however in experiments with a benchmark nonlinear problem (driven cavity), this stabilization was found to be especially important, if calculations are based on the form of equations with Bernoulli (total) pressure (2). We see the reason in the fact that for this problem the Bernoulli pressure appears to be more "substantial" variable compared to the kinematic pressure.
(c) Preconditioned iterations to solve the linearized Navier–Stokes problem. A specially designed preconditioner is used in the iterations. Moreover we will see that the stabilization mentioned in item (b) is important for a superior behavior of this linear solver.

Apart from the theory, numerical experiments for several problems are documented in detail. One problem has analytical solution, another one is the driven-cavity problem for moderate and high Reynolds numbers, the third one is "1:2" backward facing step problem with $Re = 150$ and $Re = 800$. Most important *results* and *conclusions* are summarized in the final section.

2. The problem and FE method

Let Ω be a bounded polygonal domain in R^N, $N = 2, 3$. We consider the steady incompressible Navier–Stokes equations in the *convection* form: Find a vector function $\mathbf{u}(\mathbf{x})$ (velocity) and a scalar function $p(\mathbf{x})$ (kinematic pressure) from

$$\begin{aligned} &-\nu\Delta\mathbf{u} + (\mathbf{u}\cdot\nabla)\mathbf{u} + \nabla p = \mathbf{f} \quad \text{in } \Omega, \\ &\operatorname{div}\mathbf{u} = 0 \quad \text{in } \Omega \end{aligned} \tag{1}$$

with given force field $\mathbf{f}$ and viscosity $\nu > 0$. Some boundary conditions should be additionally supplied (e.g., for velocity or stress tensor, but not solely for pressure cf. [22]). Throughout this section we assume homogeneous Dirichlet boundary conditions: $\mathbf{u} = 0$ on $\partial\Omega$.

We also consider the *rotation* form of the Navier–Stokes problem:

$$\begin{aligned} &-\nu\Delta\mathbf{u} + (\operatorname{curl}\mathbf{u})\times\mathbf{u} + \nabla P = \mathbf{f} \quad \text{in } \Omega, \\ &\operatorname{div}\mathbf{u} = 0 \quad \text{in } \Omega. \end{aligned} \tag{2}$$

The equivalence of these two formulations follows from the relation

$$(\mathbf{u}\cdot\nabla)\mathbf{u} = (\operatorname{curl}\mathbf{u})\times\mathbf{u} + \tfrac{1}{2}\nabla(\mathbf{u}^2) \tag{3}$$

with $\mathbf{u}^2 := u_1^2 + \cdots + u_N^2$. Thus the pressure distributions differ in these formulations. The Bernoulli pressure P in (2) and the kinematic pressure p in (1) are tied by

$$P = p + \tfrac{1}{2}\mathbf{u}^2. \tag{4}$$

The velocity field recovered in (1) and (2) is the same.

Given conforming FE spaces $\mathbf{U}_h \subset \mathbf{H}_0^1(\Omega)$ and $Q_h \subset L_2^0(\Omega)$, the Galerkin FE discretization of (1) or (2) is straightforward: Find $\{\mathbf{u}_h, p_h\} \in \mathbf{U}_h \times Q_h$ from

$$\nu(\nabla\mathbf{u}_h, \nabla\mathbf{v}_h) + N(\mathbf{u}_h, \mathbf{u}_h, \mathbf{v}_h) - (p_h, \operatorname{div}\mathbf{v}_h) + (q_h, \operatorname{div}\mathbf{u}_h) = (\mathbf{f}, \mathbf{v}_h) \quad \forall \mathbf{v}_h \in \mathbf{U}_h, q_h \in Q_h, \tag{5}$$

where $N(\mathbf{a}, \mathbf{u}, \mathbf{v})$ is either $((\mathbf{a}\cdot\nabla)\mathbf{u}, \mathbf{v})$ or $((\operatorname{curl}\mathbf{a})\times\mathbf{u}, \mathbf{v})$, depending on a form of equations used. Contrary to continuous case different forms of the equations in the FE scheme (5) may give different velocities $\mathbf{u}_h$: relation (3) does not hold on the FE level unless $\mathbf{u}_h^2 \in Q_h$, the latter is not the case for any standard $\mathbf{U}_h/Q_h$ FE pair. For the rotation form the conservation principle is readily fulfilled on a finite element level thanks to the property of the vector product operation: $N(\mathbf{u}_h, \mathbf{u}_h, \mathbf{u}_h) = 0$, which implies

$$\nu\|\nabla\mathbf{u}_h\|^2 = (\mathbf{f}, \mathbf{u}_h). \tag{6}$$

Here and further $\|\cdot\|$ denotes the L_2 norm and $\|\nabla\mathbf{v}\| = \left(\sum_{i,j=1}^N \|\partial u_i/\partial x_j\|^2\right)^{1/2}$. For the convection form conservation can be ensured by setting $N(\mathbf{a}, \mathbf{u}, \mathbf{v}) = 1/2\{((\mathbf{a}\cdot\nabla)\mathbf{u}, \mathbf{v}) - ((\mathbf{a}\cdot\nabla)\mathbf{v}, \mathbf{u})\}$, leading however to extra computations.

There are several critical issues associated with the Galerkin FE method. One is the compatibility of $\mathbf{U}_h$ and Q_h, i.e. the validation of the LBB (infsup) stability condition (see, e.g., [24]). LBB condition guarantees that the FE velocity space is rich enough, comparing to FE pressure space, ensuring well-posedness and full approximation order for the FE linear problem. In numerical experiments in the paper we used P1isoP2/P0

FE pair (piecewise-constant pressure and piecewise-linear continuous velocity on 2-times finer triangulation), which is LBB stable [24]: There exists mesh-independent constant $\mu(\Omega)$, such that

$$\inf_{q_h\in Q_h}\sup_{\mathbf{v}_h\in\mathbf{U}_h}\frac{(q_h,\operatorname{div}\mathbf{v}_h)}{\|\nabla\mathbf{v}_h\|\|q_h\|}=\mu_h\geqslant\mu(\Omega)>0. \tag{7}$$

It is well known that the Galerkin FE method gives optimal convergence results for elliptic problems. Thus for low order finite elements, which we used, theorem 4.2 from Chapter IV in [20] ensures $\mathrm{O}(h^2)$ asymptotic convergence of $\|\mathbf{u}-\mathbf{u}_h\|$ and $\mathrm{O}(h)$ of $\|p-p_h\|$ provided that some assumptions on regularity of $\mathbf{u}$, p and Ω are valid. However, if a continuous problem losses its ellipticity, as happens with (1) or (2) as $\nu\to 0$, the accuracy of the FE solution may deteriorate and the asymptotic convergence may be feasible for very fine meshes only. Therefore reasonable discrete solutions become available with a mesh, which resolve a stiff physical behavior of a continuous solution. Such a mesh may be prohibitively fine for practical computations, for this reason upwind, Petrov–Galerkin, or least-squares methods are popular, since they enhance stability (ellipticity) of the discrete system, preserving (hopefully) approximation properties. In some numerical experiments we will use the SUPG method. Additionally in the next section we go into some details of what we call "∇div"-stabilization. Although this alteration of the basic Galerkin method (5) is not new and can be found in [13,17,33,46], we concentrate on this issue for the following reasons: Neither physical nor numerical contents of it seems has been clearly understood; The cited references give different recipes for choosing "optimal" parameter, leaving unclear whether this additional term plays a key role or is introduced for technical reasons only; We will see in theory and numerical experiments a positive effect *both* on solution accuracy *and* the solver performance; For the equations in the rotation form this stabilization was found to be necessary already for driven cavity problem with $Re=400$.

2.1. ∇div—stabilization

Consider as a model the Stokes problem:

$$\begin{aligned}&-\nu\Delta\mathbf{u}+\nabla p=\mathbf{f}\quad\text{in }\Omega,\\&\operatorname{div}\mathbf{u}=0\quad\text{in }\Omega.\end{aligned} \tag{8}$$

The FE scheme for this problem reads: Find $\{\mathbf{u}_h,p_h\}\in\mathbf{U}_h\times Q_h$ solving

$$\nu(\nabla\mathbf{u}_h,\nabla\mathbf{v}_h)+\gamma(\operatorname{div}\mathbf{u}_h,\operatorname{div}\mathbf{v}_h)+(p_h,\operatorname{div}\mathbf{v}_h)-(q_h,\operatorname{div}\mathbf{u}_h)=(\mathbf{f},\mathbf{v}_h)\quad\forall\{\mathbf{v}_h,q_h\}\in\mathbf{U}_h\times Q_h. \tag{9}$$

The parameter $\gamma\geqslant 0$ is a stabilization parameter, which role is underpined by the error estimate in the theorem below and numerical experiments in Section 4. Since the term $\gamma(\operatorname{div}\mathbf{u}_h,\operatorname{div}\mathbf{v}_h)$ in (9) can be viewed as adding the consistent term $\gamma\nabla\operatorname{div}\mathbf{u}$ to the momentum equation in (8), we call (9) the ∇div-stabilized scheme. Although this term is consistent for continuous equations, the finite element solution depends on a value of γ. As we will see, too large values of γ "overstabilize" the problem and make corresponding linear algebraic system poor conditioned. The question of an optimal γ will be addressed further.

Theorem 1. *Assume that U_h and Q_h are such that μ_h from* (7) *is positive. Denote $\beta=\max\{\nu,\gamma\}$. The following error estimate holds*

$$\begin{aligned}&\nu\|\nabla(\mathbf{u}-\mathbf{u}_h)\|^2+\gamma\|\operatorname{div}(\mathbf{u}-\mathbf{u}_h)\|^2+\frac{\mu_h^2}{\beta}\|p-p_h\|^2\\&\quad\leqslant C\left(\inf_{\phi\in\mathbf{U}_h}\left\{\nu\|\nabla(\mathbf{u}-\phi)\|^2+\left(\gamma+\frac{\beta}{\mu_h^2}\right)\|\operatorname{div}(\mathbf{u}-\phi)\|^2\right\}+\frac{1}{\beta}\inf_{\psi\in Q_h}\|p-\psi\|^2\right)\end{aligned} \tag{10}$$

with some constant $C>0$ independent of $\mathbf{u}$, p, and all parameters of the problem.

Proof. We prove (10) in three steps. Not mentioning explicitly, we use the inequality $\|\operatorname{div}\mathbf{v}\| \leqslant \|\nabla\mathbf{v}\|$ for any $\mathbf{v} \in \mathbf{H}_0^1$. Denote also

$$a(\mathbf{u},p;\mathbf{v},q) := \nu(\nabla\mathbf{u},\nabla\mathbf{v}) + \gamma(\operatorname{div}\mathbf{u},\operatorname{div}\mathbf{v}) + (p,\operatorname{div}\mathbf{v}) - (q,\operatorname{div}\mathbf{u}),$$
$$|||\mathbf{v},q||| := \sqrt{\nu\|\nabla\mathbf{v}\|^2 + \gamma\|\operatorname{div}\mathbf{v}\|^2 + (\mu_h^2/2\beta)\|q\|^2} \quad \forall\{\mathbf{v},q\} \in \mathbf{H}_0^1 \times L_2^0.$$

Step 1 (*stability estimate*). First we show that for arbitrary $\{\mathbf{e}_h, r_h\}$ from $\{\mathbf{U}_h \times Q_h\}$ there exists a pair $\{\mathbf{v}_h, q_h\}$ such that

$$a(\mathbf{e}_h,r_h;\mathbf{v}_h,q_h) \geqslant \frac{1}{4}|||\mathbf{e}_h,r_h|||\,|||\mathbf{v}_h,q_h|||. \tag{11}$$

Condition (7) enables us to consider $\mathbf{z}_h \in \mathbf{U}_h$ such that $\|\nabla\mathbf{z}_h\| = \|r_h\|$ and $(r_h,\operatorname{div}\mathbf{z}_h) \geqslant \mu_h\|r_h\|\|\nabla\mathbf{z}_h\|$. Then an appropriate choice of $\{\mathbf{v}_h, q_h\}$ in (11) can be $\mathbf{v}_h = \mathbf{e}_h + (\mu_h/2\beta)\mathbf{z}_h$, $q_h = r_h$. Indeed, via Young's inequality we get

$$a(\mathbf{e}_h,r_h;\mathbf{e}_h,r_h) \geqslant \nu\|\nabla\mathbf{e}_h\|^2 + \gamma\|\operatorname{div}\mathbf{e}_h\|^2,$$
$$a(\mathbf{e}_h,r_h;\mathbf{z}_h,0) \geqslant \frac{\mu_h}{2}\|r_h\|^2 - \frac{\nu^2}{\mu_h}\|\nabla\mathbf{e}_h\|^2 - \frac{\gamma^2}{\mu_h}\|\operatorname{div}\mathbf{e}_h\|^2.$$

We multiply the second inequality by $\mu_h/2\beta$ and add it to the first one. This leads to

$$a\left(\mathbf{e}_h,r_h;\mathbf{e}_h + \frac{\mu_h}{2\beta}\mathbf{z}_h,q_h\right) \geqslant \frac{\nu}{2}\|\nabla\mathbf{e}_h\|^2 + \frac{\gamma}{2}\|\operatorname{div}\mathbf{e}_h\|^2 + \frac{\mu_h^2}{4\beta}\|r_h\|^2 \geqslant \frac{1}{2}|||\mathbf{e}_h,r_h|||^2.$$

Now to prove inequality (11) we need to show

$$|||\mathbf{v}_h,q_h||| \leqslant 2|||\mathbf{e}_h,r_h|||.$$

The latter is easy to see, thanks to the definition of $q_h = r_h$ and $\mathbf{v}_h = \mathbf{e}_h + (\mu_h/2\beta)\mathbf{z}_h$, and

$$\left|\left|\left|\frac{\mu_h}{2\beta}\mathbf{z}_h,0\right|\right|\right|^2 = \frac{\mu_h^2}{4\beta^2}(\nu\|\nabla\mathbf{z}_h\|^2 + \gamma\|\operatorname{div}\mathbf{z}_h\|^2) \leqslant \frac{\mu_h^2}{2\beta}\|r_h\|^2 \leqslant |||\mathbf{e}_h,r_h|||^2.$$

Step 2 (*continuity estimate*). From the Cauchy inequality we get for any $\{\mathbf{e},r\}$ and $\{\mathbf{v},q\}$ from $\mathbf{H}_0^1(\Omega) \times L_2^0$

$$\begin{aligned} a(\mathbf{e},r;\mathbf{v},q) &\leqslant \nu\|\nabla\mathbf{e}\|\|\nabla\mathbf{v}\| + \gamma\|\operatorname{div}\mathbf{e}\|\|\operatorname{div}\mathbf{v}\| + \|r\|\|\operatorname{div}\mathbf{v}\| \\ &\quad + \|q\|\|\operatorname{div}\mathbf{e}\| \leqslant \sqrt{\nu\|\nabla\mathbf{e}\|^2 + \left(\gamma + \frac{\beta}{\mu_h^2}\right)\|\operatorname{div}\mathbf{e}\|^2 + \frac{1}{\beta}\|r\|^2}\sqrt{2(\nu\|\nabla\mathbf{v}\|^2 + \gamma\|\operatorname{div}\mathbf{v}\|^2) + \frac{\mu_h^2}{\beta}\|q\|^2} \\ &= \sqrt{2}\sqrt{\nu\|\nabla\mathbf{e}\|^2 + \left(\gamma + \frac{\beta}{\mu_h^2}\right)\|\operatorname{div}\mathbf{e}\|^2 + \frac{1}{\beta}\|r\|^2}|||\mathbf{v},q||| = \sqrt{2}\ell(\mathbf{e},r)|||\mathbf{v},q|||. \end{aligned} \tag{12}$$

Here we denote

$$\ell(\mathbf{e},r) = \sqrt{\nu\|\nabla\mathbf{e}\|^2 + \left(\gamma + \frac{\beta}{\mu_h^2}\right)\|\operatorname{div}\mathbf{e}\|^2 + \frac{1}{\beta}\|r\|^2}.$$

Step 3. Let $\mathbf{e}_h = \mathbf{u}_h - \phi$, $r_h = p_h - \psi$ and $\mathbf{e} = \mathbf{u} - \phi$, $r = p - \psi$ for some arbitrary $\phi \in \mathbf{U}_h$ and $\psi \in Q_h$. The Galerkin orthogonality implies

$$a(\mathbf{e}_h,r_h;\mathbf{v}_h,q_h) = a(\mathbf{e},r;\mathbf{v}_h,q_h) \quad \forall\{\mathbf{v}_h,q_h\} \in \mathbf{U}_h \times Q_h. \tag{13}$$

Stability estimate (11), (13), and (12) with $\mathbf{v} = \mathbf{v}_h$, $q = q_h$ enables us to estimate $|||\mathbf{e}_h, r_h||| \leqslant 4\sqrt{2}\ell(\mathbf{e}, r)$. Since $\mu_h \leqslant 1$, we also have $|||\mathbf{e}, r||| \leqslant \ell(\mathbf{e}, r)$. Therefore, thanks to triangle inequality we get the result

$$|||\mathbf{u} - \mathbf{u}_h, p - p_h||| \leqslant |||\mathbf{e}_h, r_h||| + |||\mathbf{e}, r||| \leqslant (4\sqrt{2} + 1)\ell(\mathbf{e}, r). \tag{14}$$

Since ϕ and ψ in the definition of $\mathbf{e}$ and r are arbitrary functions from $\mathbf{U}_h$ and Q_h, we can take infimum in the r.h.s. in (14) over these spaces. Therefore we arrive at (10) with $C = (4\sqrt{2} + 1)^2$ after squaring. □

The theorem can be applied to draw convergence estimates for a particular LBB-stable finite element pair as in the example below.

Example 1. Assume the solution to the Stokes problem (8) is smooth enough and the mesh is quasi-regular, then for P1isoP2/P0 finite elements we have

$$v\|\nabla(\mathbf{u} - \mathbf{u}_h)\|^2 + \frac{\mu_h^2}{\beta}\|p - p_h\|^2 \leqslant Ch^2\left(\beta\left(1 + \frac{1}{\mu_h^2}\right)\|\mathbf{u}\|_{H^2}^2 + \frac{1}{\beta}\|p\|_{H^1}^2\right). \tag{15}$$

To see the predicted effect of introducing γ-term suppose that the problem (8) has a non-trivial continuous pressure solution ($p \notin Q_h$) and suppose for a moment that $\mathbf{u}$ and p are independent of v, then for $\gamma = 0$ the estimate (15) ensures only

$$\|\nabla(\mathbf{u} - \mathbf{u}_h)\| \leqslant \frac{c(h)}{v}, \tag{16}$$

while for $\gamma = \mathrm{O}(1)$

$$\|\nabla(\mathbf{u} - \mathbf{u}_h)\| \leqslant \frac{c(h)}{\sqrt{v}}, \tag{17}$$

where a constant $c(h)$ depends on approximation properties of FE spaces and p, but not on v. Moreover for $\gamma = \mathrm{O}(1)$ the following natural norm of the error

$$|[\mathbf{u} - \mathbf{u}_h, p - p_h]| := \sqrt{v\|\nabla(\mathbf{u} - \mathbf{u}_h)\|^2 + \|p - p_h\|^2} \tag{18}$$

is controlled independently of v, although this norm becomes weak for velocity if $v \to 0$. Of course, in 'real' problems both $\mathbf{u}$ and p are v-dependent, and therefore their norms involved in standard approximation estimates, say $\|\mathbf{u}\|_{H_2}$ and $\|p\|_{H_1}$, can be v-dependent too. For the Navier–Stokes problem this dependence is hard to predict. A standard regularity theory for the equations suggests $\|\mathbf{u}\|_{H^k} \sim \|p\|_{H^{k-1}}$. At the same time theory from this section, in particular (16) and (17), is well supported by numerical experiments not only for the Stokes problem, but also for the linearized Navier–Stokes problem. Experiments with nonlinear problem also clearly show that ∇div-stabilization improves accuracy for carefully chosen parameter γ. Example 1 illustrates that this stabilization intends to suppress instabilities induced by the pressure, whenever $\|p\|_{H^1}$ is noticeable.

The estimate (10) hints also the best choice of the stabilization parameter. Consider first the case when an approximation of velocity is one degree larger than of pressure (e.g., P1isoP2–P0, non-conforming P1–P0, P2–P1 FE pairs), then a balance of the last two terms in (10) gives the choice $\gamma \sim \mu_h$ for $v \leqslant \mu_h$ and $\gamma = 0$ otherwise. In the case of equal order approximation (e.g., P1isoP2–P1 FE pair) the best choice is $\gamma \sim \mu_h h$ for $v \leqslant \mu_h h$, however provided that the pressure is sufficiently smooth: $\|p\|_{H^2}$ is reasonably bounded. Numerical experiments with P1isoP2–P0 FE pair in the paper confirm the above choice. For some simple domains quite accurate estimates of μ_h are known (see [11]). Moreover numerical experiments in [11] show that μ_h does not depend on the anisotropy of triangulation for P1isoP2–P0 elements, see [1] for the coverage of some other finite elements pairs.

2.2. SUPG stabilization

Another potential source of instabilities in (1) is dominating convection terms. This enforces one to stabilize a discrete system if a mesh is not sufficiently fine. We briefly outline the SUPG method we implemented. Much more details on this family of stabilization methods can be found in [9,13,17,33], and references therein.

The Navier–Stokes equations in convection form (1) is a starting point, further a weighted residual for FE solution is added to the Galerkin scheme (5) multiplied by a solution-depended test function:

$$\begin{aligned}&\nu(\nabla\mathbf{u}_h,\nabla\mathbf{v}_h)+N(\mathbf{u}_h,\mathbf{u}_h,\mathbf{v}_h)-(p_h,\operatorname{div}\mathbf{v}_h)+(q_h,\operatorname{div}\mathbf{u}_h)\\&\quad+\sum_{\tau\in T_h}\sigma(\tau,\mathbf{u}_h)(-\nu\Delta\mathbf{u}_h+\mathbf{u}_h\cdot\nabla\mathbf{u}_h+\nabla p_h-\mathbf{f},\mathbf{u}_h\cdot\nabla\mathbf{v}_h)_\tau=(\mathbf{f},\mathbf{v}_h)\quad\forall\mathbf{v}_h\in\mathbf{U}_h,q_h\in Q_h,\end{aligned}\tag{19}$$

The "new" term in (19) is evaluated element-wise for each element τ of a triangulation T_h. A parameter $\sigma(\tau,\mathbf{u}_h)$ is element and solution-dependent. Several recommendations can be found in literature for the choice of $\sigma(\tau,\mathbf{u}_h)$. The general idea is to add almost no additional stabilization terms in regions of small mesh Reynolds numbers, hence to recover 'optimal' Galerkin method by setting $\sigma(\tau)\ll 1$ (or even $\sigma(\tau)=0$) in these regions, but to add these terms in regions of large mesh Reynolds numbers. However, the particular choice of $\sigma(\tau,\mathbf{u}_h)$ is still a matter of discussion. We use the one from [33] and [44], see also [34]:

$$\sigma(\tau,\mathbf{u}_h)=\sigma\frac{h_\tau}{\|\mathbf{u}\|_\Omega}\frac{2Re_\tau}{1+Re_\tau},\qquad Re_\tau:=\frac{\|\mathbf{u}\|_{L_2(\tau)}h_\tau}{\nu}.\tag{20}$$

This choice is provided by the minimization of an a priori error estimate for the discrete solution of (19) and was successfully tested in many numerical experiments in [44].

In our experiments we take either $\sigma=0.2$ or $\sigma=0$, the latter means that no SUPG terms are added. For isotropic meshes h_τ represents a diameter of element τ. In the case of anisotropic meshes h_τ can be chosen as an "effective" mesh size: An element diameter in a flow direction [18]. Another analysis for anisotropic grids is found in [2].

Since we use piecewise-linear approximation for velocity and piecewise-constant for pressure, viscous and pressure terms disappear from FE residual in (19) and the method amounts in adding $\sum_{\tau\in T_h}\sigma(\tau,\mathbf{u}_h)(\mathbf{u}_h\cdot\nabla\mathbf{u}_h,\mathbf{u}_h\cdot\nabla\mathbf{v}_h)_\tau$ to momentum equations. If $\mathbf{f}\neq 0$, then the extra $\mathbf{f}$-dependent term is also added.

In our numerical experiments SUPG method will be used for calculating high-*Re* flows and only with convection form of equations.

3. Solvers

To illustrate ideas that are fairly standard we will occasionally use "continuous" notations in this section. When details are important we will operate with matrices and vectors of nodal values. To solve nonlinear problem the fix-point defect correction method is applied: Given iterate $\{\mathbf{u}^m,p^m\}$ and relaxation parameter $\omega>0$ find $\{\mathbf{u}^{m+1},p^{m+1}\}$ from

$$\begin{pmatrix}\mathbf{u}^{m+1}\\p^{m+1}\end{pmatrix}=\begin{pmatrix}\mathbf{u}^{m}\\p^{m}\end{pmatrix}-\omega\mathrm{LNS}(\mathbf{u}^m)^{-1}\begin{pmatrix}-\nu\Delta\mathbf{u}^m-\gamma\nabla\operatorname{div}\mathbf{u}^m+N(\mathbf{u}^m,\mathbf{u}^m)+\nabla p^m-\mathbf{f}\\-\operatorname{div}\mathbf{u}^m\end{pmatrix},\tag{21}$$

where $N(\mathbf{u}^m,\mathbf{u}^m)=\operatorname{curl}\mathbf{u}^m\times\mathbf{u}^m$ or $=\mathbf{u}^m\cdot\nabla\mathbf{u}^m$. For $\sigma>0$ the SUPG terms are also included to compute the defect in (21). $\mathrm{LNS}(\mathbf{u}^m)^{-1}$ is a solution operator to the linearized Navier–Stokes equations. This iterations are quite robust for the problem in the convection form [44], especially if stabilizing terms are added. However we found that for the rotation form iterations (21) are not so robust for small ν. Thus in the case of the rotation form we use implicit BE method. Then on every "time" step of BE one arrives at nonlinear problem similar to (1) or (2) with additional reactive term $(1/\delta t)\mathbf{u}$ in the momentum equations. To solve this new nonlinear problem we perform few iterations (21), taking velocity from the previous time as an initial guess.

The linearized problem to be solved on each iteration (21) reads: Given $\mathbf{u}^m$ and $\mathrm{res}_{\mathbf{u}}^m$ find $\{\mathbf{v}, q\}$ from

$$\begin{aligned}&\frac{1}{\delta t}\mathbf{v} - \nu\Delta\mathbf{v} - \gamma\nabla\operatorname{div}\mathbf{v} + N(\mathbf{u}^m, \mathbf{v}) + \nabla q = \mathrm{res}_{\mathbf{u}}^m \quad \text{in } \Omega,\\ &-\operatorname{div}\mathbf{v} = -\operatorname{div}\mathbf{u}^m \quad \text{in } \Omega,\\ &\text{homogenuous } b.c. \text{ on } \partial\Omega,\end{aligned} \tag{22}$$

where $N(\mathbf{u}^m, \mathbf{v}) = \operatorname{curl}\mathbf{u}^m \times \mathbf{v}$ for the rotation form and $N(\mathbf{u}^m, \mathbf{v}) = (\mathbf{u}^m \cdot \nabla)\mathbf{v}$ for the convection one. If the SUPG method is used for nonlinear problems, then the SUPG term is linearized in the natural way: $\sum_\tau \sigma(\tau, \mathbf{u}^m)(\mathbf{u}^m \cdot \nabla\mathbf{v}_h, \mathbf{u}^m \cdot \nabla\mathbf{w}_h)_\tau$ and included in the FE formulation of (22). This additional term is symmetric and non-negative.

Note that the linearization of equations in rotation form results in the 0-order term $(\operatorname{curl}\mathbf{u}^m) \times \mathbf{v}$ in (22), comparing to the 1st-order of $(\mathbf{u}^m \cdot \nabla)\mathbf{v}$ in convection form. In both cases the linearized equations preserve ellipticity and conservation property (6).

3.1. Linear solver

Problem (22) is linear, however non-symmetric and of saddle-point type. Therefore a special technique is required to treat it. To solve (22) we use *coupled iterations*, i.e. pressure and velocity are iterated together. Several methods of this type can be found in the literature. Often direct multi-grid methods are used (e.g. [25,45,51,52]). Discussion of advantages and disadvantages of such methods and further references can be found in [50]. Trying to avoid particular problems associated with building a multigrid for saddle-point problem, more recently preconditioned methods based on outer–inner iteration, which have a long history [4] for symmetric saddle-point problems, were adopted for non-symmetric ones (e.g., [8,16,37,43]). It is not our intention here to compare these different approaches, see results of this type for symmetric case in [14]. Below we consider preconditioned method based on outer–inner iterations with particular attention to the case of $\nu \to 0$.

Let A and B be matrices stemming from a FE method applied to (22): For any basic nodal functions $\psi_i, \psi_j \in \mathbf{U}_h$ and $\phi_k \in Q_h$ the entries of matrices A and B are defined by

$$\begin{aligned}&A_{i,j} = \nu(\nabla\psi_j, \nabla\psi_i) + \gamma(\operatorname{div}\psi_j, \operatorname{div}\psi_i) + \left(\frac{1}{\delta t}\psi_j + N(\mathbf{u}^m, \psi_j), \psi_i\right) + \sum_{\tau\in T_h}\sigma(\tau, \mathbf{u}^m)(\mathbf{u}^m \cdot \nabla\psi_j, \mathbf{u}^m \cdot \nabla\psi_i)_\tau,\\ &B_{k,i} = -(\operatorname{div}\psi_i, \phi_k).\end{aligned}$$

With these notations one has to solve the system of linear algebraic equations:

$$\begin{pmatrix} A & B^{\mathrm{T}} \\ B & 0 \end{pmatrix}\begin{pmatrix} x \\ y \end{pmatrix} = \begin{pmatrix} f \\ g \end{pmatrix}. \tag{23}$$

The spectrum of the matrix from (23) contains eigenvalues with both positive and negative real parts and its condition number strongly depends on the mesh-size and ν ([16,37,48]), leading to a poor conditioning as $h \to 0$ and/or $\nu \to 0$. Thus to solve (23) iteratively a preconditioning is highly desirable. Let $\hat{A}$ be a preconditioner for A and $\hat{S}$ a preconditioner for S, the Schur complement of the system:

$$S := BA^{-1}B^{\mathrm{T}}.$$

Using a pattern from [30], the block triangular preconditioner for (23) is defined as

$$\mathscr{P}^{-1} = \begin{pmatrix} \hat{A}^{-1} & \hat{A}^{-1}B^{\mathrm{T}}\hat{S}^{-1} \\ 0 & -\hat{S}^{-1} \end{pmatrix}. \tag{24}$$

If $\hat{A} = A$ and $\hat{S} = S$, then a preconditioned Krylov subspace method for (23) will converge in at most two iterations. Generally, we are looking for $\hat{A}$ and $\hat{S}$ to be close to A and S, but such that $\hat{A}^{-1}x$ and $\hat{S}^{-1}y$ can be "easily" computed for given vectors x and y. Convergence analysis of the GMRES method with this preconditioning is given in [30]. We use the BiCGstab method [47] to iterate the following preconditioned system up to a desirable tolerance:

$$\begin{pmatrix} A & B^{\mathrm{T}} \\ B & 0 \end{pmatrix} \begin{pmatrix} \hat{A}^{-1} & \hat{A}^{-1}B^{\mathrm{T}}\hat{S}^{-1} \\ 0 & -\hat{S}^{-1} \end{pmatrix} \begin{pmatrix} \hat{x} \\ \hat{y} \end{pmatrix} = \begin{pmatrix} f \\ g \end{pmatrix}. \tag{25}$$

Two essential ingredients: $\hat{A}$ and $\hat{S}$ are remaining to be defined. First let us consider the rotation form. In doing this we use some ideas from [37,38]. $\hat{A}$ is a preconditioner for the pure velocity problem. The continuous counterpart of this problem reads

$$\begin{aligned} &\alpha\mathbf{v} - \nu\Delta\mathbf{v} - \gamma\nabla\operatorname{div}\mathbf{v} + w \times \mathbf{v} = \text{r.h.s} \quad \text{in } \Omega, \\ &\text{homogenuous } b.c. \quad \text{on } \partial\Omega \end{aligned} \tag{26}$$

with $w = \operatorname{curl}\mathbf{u}^m$, $\alpha = 1/\delta t$. Compared to the convection–diffusion vector problem that appears, if one linearize the Navier–Stokes equations in convection form, Eq. (26) has 2nd-order and 0-order terms only. This allows *standard* multi-grid components to work well and to solve a FE approximation of Eq. (26). Multi-grid components include a block Jacobi or block Gauss–Seidel iteration as smoother. The robustness of the multi-grid as a solver was proved in [38] for the case $\gamma = 0$. At the same time, if $\gamma = O(1)$ and $\nu, \alpha \to 0$, the problem (26) has anisotropic diffusion terms and may have a large kernel in the limit case $\nu = 0$ and $\alpha = 0$, therefore the performance of standard multi-grid tools deteriorates. Fortunately, as we will see from numerical experiments, for the realistic values of ν, a loss in convergence is not dramatic and we have a hope that specially designed smoothing and prolongation operators can further improve the situation. We summarize all these, saying that for $\hat{A}^{-1}$ we take few V-cycles of the multi-grid method applied to solve FE system approximating (26).

Demand for a preconditioner to the Schur complement S is the price we pay for the desire to solve "true" coupled systems like (1) or (2), rather then to decouple somehow pressure from the original system [39]. Matrix S is a dense matrix: Most entries are non-zero and cannot be computed in a straightforward (economical) manner. Therefore, non-standard considerations have to be made to build $\hat{S}$. Below we present a particular choice of $\hat{S}$ and some analysis aimed to predict the robustness of this choice follows. Let M_{p} be a mass matrix for the pressure FE space and $\hat{M}_{\mathrm{p}}$ its diagonal lumping, then

$$\hat{S}^{-1} = (\nu + \gamma)\hat{M}_{\mathrm{p}}^{-1} + S_0(w)^{-1}, \tag{27}$$

where $S_0(w) := B\hat{M}_u(w)^{-1}B^{\mathrm{T}}$ is a Schur complement of

$$\begin{pmatrix} \hat{M}_u(w) & B^{\mathrm{T}} \\ B & 0 \end{pmatrix}, \quad \text{where in two-dimensional case } \hat{M}_u(w) = \begin{pmatrix} \alpha\hat{M}_u & -\hat{M}_u^w \\ \hat{M}_u^w & \alpha\hat{M}_u \end{pmatrix}, \tag{28}$$

$\hat{M}_u$ is a lumped velocity mass matrix and $\hat{M}_u^w$ is a lumped mass-type matrix, corresponding to the w-weighted scalar product $\int_\Omega w(\mathbf{x})u(\mathbf{x})v(\mathbf{x})\,\mathrm{d}\mathbf{x}$. For further clarity we note that (28) can be viewed as the matrix of a discrete counterpart of the following reduced ($\nu = 0$, $\gamma = 0$) problem Eq. (22):

$$\begin{aligned}&\alpha\mathbf{v}+w\times\mathbf{v}+\nabla q=\text{r.h.s.}\quad\text{in }\Omega,\\&-\operatorname{div}\mathbf{v}=\text{r.h.s.}\quad\text{in }\Omega,\\&\text{homogenous } b.c. \text{ for } \mathbf{v}\cdot\mathbf{n}\quad\text{on }\partial\Omega,\quad \mathbf{n}-\text{normal vector to }\partial\Omega.\end{aligned}\tag{29}$$

In the three-dimensional case $\hat{M}_u(w)$ is a 3×3 block matrix. The Schur complement $S_0(w)$ of the reduced problem is now a *sparse* matrix that mimics a mixed discretization for the pressure-Poisson problem. Therefore, a multi-grid method is a good candidate to evaluate $S_0(w)^{-1}$. In fact, few multi-grid V-cycles will suffice for our needs.

Important to note that problem (29) (resp. (28)) can be ill-posed for $\alpha = 0$. Two decisions can be made for small α. The first, which we commonly take, is to add $S_0(w)^{-1}$ to (27) only if $\alpha \geqslant \bar{\alpha}$. We take $\bar{\alpha} = 1$ in the experiments. However, if $\alpha = 0$ and $\gamma = 0$ the analysis in the next section predicts that artificial $\bar{\alpha} \sim \|w\|$ is a useful choice for the case of a small viscosity. We will call $\hat{S}$ with $\bar{\alpha}$—a modified Schur complement preconditioner.

For the Navier–Stokes equations in convection form the linearization leads to system (23). Now A stands for a matrix corresponding to a discretization of the vector convection–diffusion problem (with the reactive term and anisotropic diffusion):

$$\begin{aligned}&\alpha\mathbf{v}-\nu\Delta\mathbf{v}-\gamma\nabla\operatorname{div}\mathbf{v}+(\mathbf{a}\cdot\nabla)\mathbf{v}=\text{r.h.s}\quad\text{in }\Omega,\\&\text{homogenuous } b.c.\quad\text{on }\partial\Omega,\end{aligned}\tag{30}$$

with $\mathbf{a} = \mathbf{u}^m$. If $\gamma = 0$, then the system (30) splits into two scalar convection–diffusion problems. For a FE approximation of the latter multi-grid methods are known to be a good choice as solvers. We use a geometric multi-grid method to build a preconditioner $\hat{A}$. Smoother, grid transfer operators, and coarse-grid matrices are the main ingredients to be defined. We found that for *stabilized* equations the appropriate choice was standard (induced by the embeddings $U_{2h} \subset U_h$ and $P_{2h} \subset P_h$) 1st-order projection and restriction, alternating Gauss-Seidel method with lexicographical ordering of unknowns as a smoother, and a FE approximation of (30) on a coarse grid as the coarse-grid problem. For the coarse-grid problem we found important to define SUPG stabilization parameters correspond to the coarse grid; for a similar experience with a multi-grid method for convection–diffusion equations see [40]. For globally refined grids multi-grid methods, e.g. V- and W-cycles for two-dimensional problems lead to optimal complexity, however for locally refined grids special smoothing strategies should be used to retain optimal complexity (see, [5]).

A proper preconditioner for the Schur complement S in the convection form is a challenging problem. Recently in [15,31,43] two types of preconditioners, which take the convection into account, were proposed. They were derived with assumptions on convection $\mathbf{a}$ to be a constant vector and boundary conditions to be periodic. Both preconditioners require the construction of operators of the convection–diffusion type on the discrete pressure space. For piecewise constant pressure this imposes certain difficulties. One possible way to overcome them [49] is to consider a dual triangulation for the pressure by connecting the centroids of the triangles in which pressure is defined. Then one can define piecewise linear and continuous pressure on the dual triangulation. Avoiding additional implementation efforts, we alternatively set $\hat{S}^{-1} = (\nu+\gamma)\hat{M}_{\mathrm{p}}^{-1}$. Numerical experiments from [31,43] show the advantage of their more sophisticated preconditioner for the case of $\gamma = 0$, this modification can be especially useful for higher order pressure approximations.

3.2. Fourier analysis

This subsection gives an analysis that explains the advantage of the choice (27) of $\hat{S}$. We consider the two-dimensional periodic case and constant $w(\mathbf{x}) = w \neq 0$.

Let us evaluate the operator S on a given harmonic $q(\mathbf{x}) = \exp(i(\mathbf{c},\mathbf{x}))$, where $\mathbf{c},\mathbf{x} \in R^2$. First we have

$$\nabla q(\mathbf{x}) = \{ic_1 \exp(i(\mathbf{c},\mathbf{x})), ic_2 \exp(i(\mathbf{c},\mathbf{x}))\}.$$

Looking for $\mathbf{u}$ of the form $u_1 = ik_1 \exp(i(\mathbf{c},\mathbf{x}))$, $u_2 = ik_2 \exp(i(\mathbf{c},\mathbf{x}))$, we find from

$$-\nu\Delta u_1 - \gamma\frac{\partial}{\partial x_1}\left(\frac{\partial u_1}{\partial x_1}+\frac{\partial u_2}{\partial x_2}\right) + \alpha u_1 - w u_2 = \frac{\partial q(\mathbf{x})}{\partial x_1},$$
$$-\nu\Delta u_2 - \gamma\frac{\partial}{\partial x_2}\left(\frac{\partial u_1}{\partial x_1}+\frac{\partial u_2}{\partial x_2}\right) + \alpha u_2 + w u_1 = \frac{\partial q(\mathbf{x})}{\partial x_2}$$

the coefficients

$$k_1 = \frac{(\alpha+\nu|\mathbf{c}|^2+\gamma c_2^2)c_1 + (\gamma c_1 c_2 + w)c_2}{(\alpha+\nu|\mathbf{c}|^2\gamma c_1^2)(\alpha+\nu|\mathbf{c}|^2\gamma c_2^2) - \gamma^2 c_1^2 c_2^2 + w^2},$$
$$k_2 = \frac{(\alpha+\nu|\mathbf{c}|^2+\gamma c_1^2)c_2 - (\gamma c_1 c_2 + w)c_1}{(\alpha+\nu|\mathbf{c}|^2\gamma c_1^2)(\alpha+\nu|\mathbf{c}|^2\gamma c_2^2) - \gamma^2 c_1^2 c_2^2 + w^2}.$$

Therefore,

$$S\exp(i(\mathbf{c},\mathbf{x})) = -\operatorname{div}\mathbf{u} = \frac{(\alpha+\nu|\mathbf{c}|^2)|\mathbf{c}|^2}{(\alpha+\nu|\mathbf{c}|^2)(\alpha+(\nu+\gamma)|\mathbf{c}|^2)+w^2}\exp(i(\mathbf{c},\mathbf{x})).$$

Let us consider the case of $\alpha = 0$. For $\alpha > 0$ *the condition number of the preconditioned system only improves* and ν-independent estimates can be obtained (see relevant analysis for the case $\gamma = 0$ in [37]). For $\alpha = 0$ we omit $S_0(w)^{-1}$ in $\hat{S}^{-1}$ and for the preconditioned problem we have

$$\hat{S}^{-1}S\exp(i(\mathbf{c},\mathbf{x})) = \frac{\nu(\nu+\gamma)|\mathbf{c}|^4}{\nu(\nu+\gamma)|\mathbf{c}|^4+w^2}\exp(i(\mathbf{c},\mathbf{x})). \tag{31}$$

This results for fine enough mesh ($|\mathbf{c}|^4$ can be large) in

$$\gamma = \mathrm{O}(1):\ \operatorname{cond}(\hat{S}^{-1}S) \sim 1 + \mathrm{O}(\nu^{-1}),\quad \nu \to 0, \tag{32}$$

$$\gamma = 0:\ \operatorname{cond}(\hat{S}^{-1}S) \sim 1 + \mathrm{O}(\nu^{-2}),\quad \nu \to 0. \tag{33}$$

The asymptotic in (33) is consistent with known results for Oseen problem [16,37]. Comparing (32) and (33), we see that the stabilized problem admits much better, although still simple, preconditioning. This result of improving the condition number for the Schur complement of the stabilized system agrees with the improvement of discrete solution accuracy, see Theorem 1. Thus, while ∇div-stabilization is consistent for the Navier–Stokes system it amounts in additional diffusion for the Schur complement of the system.

To derive further conclusions from (31) denote by λ_n the nth eigenvalue of $\hat{S}^{-1}S$ in the increasing sequence $0 < \lambda_1 < \lambda_2 < \cdots < \lambda_n < \cdots$ The eigenvalue λ_n can be of multiplicity >1 and it corresponds to some $|\mathbf{c}|^2 \geqslant n$. Now, considering separately two cases $\nu(\nu+\gamma)|\mathbf{c}|^4 \leqslant w^2$ and $\nu(\nu+\gamma)|\mathbf{c}|^4 > w^2$, it is easy to check that

$$\frac{1}{2}\min\left\{1, n^2\frac{\nu(\nu+\gamma)}{w^2}\right\} \leqslant \lambda_n \leqslant 1,\quad n = 1,2,\ldots \tag{34}$$

Therefore, besides the difference in order of smallest eigenvalues for $\gamma = 0$ and $\gamma = \mathrm{O}(1)$, the operator $\hat{S}^{-1}S$ has at most $\mathrm{O}(\nu^{-1/2})$ small eigenvalues for $\gamma = \mathrm{O}(1)$, while for $\gamma = 0$ the bound is $\mathrm{O}(\nu^{-1})$.

Numerical experiments also show that for the non-stabilized problem ($\gamma = 0$) it makes sense to include $S_0(w)^{-1}$ in the preconditioner $\hat{S}$ (see (27)) even for $\alpha = 0$, taking some auxiliary $\bar{\alpha} > 0$ in the definition of $S_0(w)$ (see (28)). The Fourier analysis confirms this fact: It is straightforward to check ($\alpha = 0, \gamma = 0$):

$$\hat{S}^{-1} S \exp(i(\mathbf{c}, \mathbf{x})) = \left(\frac{\nu^2 |\mathbf{c}|^4}{\nu^2 |\mathbf{c}|^4 + w^2} + \frac{(\bar{\alpha}^2 + w^2)\nu |\mathbf{c}|^2}{\bar{\alpha}(\nu^2 |\mathbf{c}|^4 + w^2)} \right) \exp(i(\mathbf{c}, \mathbf{x})).$$

Setting $\bar{\alpha} = |w|$, we get

$$\hat{S}^{-1} S \exp(i(\mathbf{c}, \mathbf{x})) = \frac{\nu^2 |\mathbf{c}|^4 + w\nu |\mathbf{c}|^2}{\nu^2 |\mathbf{c}|^4 + w^2} \exp(i(\mathbf{c}, \mathbf{x})).$$

Hence

$$\mathrm{cond}(\hat{S}^{-1} S) \leqslant 4 \frac{\nu^2 + w^2}{\nu^2 + w\nu} = \mathrm{O}\left(\frac{w}{\nu}\right) \quad \text{as } \frac{w}{\nu} \to \infty$$

which is better then (33) for $w = \mathrm{O}(1)$.

Since for "real" problems w is not a constant, but a function of a quite complicated behavior, numerical experiments are important to verify our conclusions.

4. Numerical experiments

Performing numerical experiments we were particularly interested in: (1) The effect of ∇div-terms on discrete solution accuracy *and* convergence of iterations; (2) The performance of linear multi-grid methods for the auxiliary velocity and pressure problem; (3) The performance of the preconditioned Krylov subspace method to solve (25) for the linearized Navier–Stokes problem; (4) The convergence of nonlinear iterations to the steady solution.

Three model problems were considered.

Problem I (*with analytical solution*). We take "exact" solution $\mathbf{u} = (u_1, u_2)$ and p as

$$\begin{aligned} u_1(x,y) &= \frac{r_2}{2\pi} \frac{\mathrm{e}^{r_2 y}}{(\mathrm{e}^{r_2} - 1)} \sin\left(\frac{2\pi(\mathrm{e}^{r_2 y} - 1)}{\mathrm{e}^{r_2} - 1}\right)\left(1 - \cos\left(\frac{2\pi(\mathrm{e}^{r_1 x} - 1)}{\mathrm{e}^{r_1} - 1}\right)\right), \\ u_2(x,y) &= -\frac{r_1}{2\pi} \frac{\mathrm{e}^{r_1 x}}{(\mathrm{e}^{r_1} - 1)} \sin\left(\frac{2\pi(\mathrm{e}^{r_1 x} - 1)}{\mathrm{e}^{r_1} - 1}\right)\left(1 - \cos\left(\frac{2\pi(\mathrm{e}^{r_2 y} - 1)}{\mathrm{e}^{r_2} - 1}\right)\right), \\ p(x,y) &= r_1 r_2 \frac{\mathrm{e}^{r_1 x}\mathrm{e}^{r_2 y}}{(\mathrm{e}^{r_1} - 1)(\mathrm{e}^{r_2} - 1)} \sin\left(\frac{2\pi(\mathrm{e}^{r_1 x} - 1)}{\mathrm{e}^{r_1} - 1}\right) \sin\left(\frac{2\pi(\mathrm{e}^{r_2 y} - 1)}{\mathrm{e}^{r_2} - 1}\right) \end{aligned} \tag{35}$$

with $r_1 = 3$, $r_2 = 0.1$ and $\Omega = (0,1) \times (0,1)$. Bernoulli pressure is computed from (4). This type of convection simulates a rotating vortex. The vortex center has coordinates (x_0, y_0), $x_0 \approxeq 0.785$, $y_0 \approxeq 0.512$. This analytical test was taken from the paper of Berrone [6], where the corresponding values of approximation errors are given for a SUPG-type scheme and P1/P1 FE pair applied to the linearized Navier–Stokes problem in convection form and both uniform and adapted grids. In our experiments the LBB stable P1isoP2/P0 finite elements are used on a uniform triangulation.

Problem II (*driven cavity*). In $\Omega = (0,1) \times (0,1)$ find $\{\mathbf{u}, p\}$ solving (2) with $\mathbf{f} = 0$ and $u_1(x,1) = 1$, $u_2(x,1) = 0$ and $\mathbf{u} = 0$ on the remainder of the boundary. This is a standard test for incompressible flow solvers and a lot of data is available for comparison.

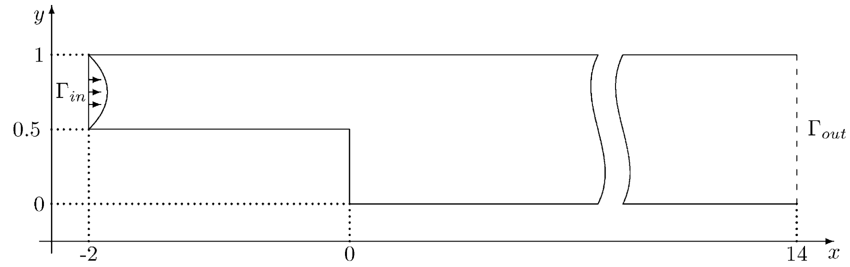

Fig. 1. Backward facing step configuration.

Problem III (*backward facing step*). Another standard test for steady Navier–Stokes equations is a flow over a backward facing step, cf. Fig. 1. We employed "h:$H = 1$:2" configuration (H is a height of the channel and h is a height of the step) with parabolic velocity profile on the inlet Γ_{in}. The average inflow is defined as

$$U = \frac{1}{|H-h|}\int_{\Gamma_{\text{in}}} u_1(-2,y)\,\mathrm{d}y.$$

The Reynolds number is $Re = UH/\nu$. On the outflow part of the boundary Γ_{out} we implement natural "do-nothing" boundary conditions, see e.g. [10], to minimize an upstream influence of the artificial outflow boundary. Both numerical and experimental results are available from literature. The steady two-dimension flow is known to be stable for the Reynolds numbers up to 800 [23].

In Table 1 we summarize the results of calculations for Problem I with different values of parameter γ. We denote $e_h = \mathbf{u} - \mathbf{u}_h$ and $q_h = p - p_h$, the norm $|[e_h, q_h]|$ was defined in (18). The positive effect of the ∇div-stabilization both w.r.t. accuracy and the total number of iterations is seen for the linearized Navier–Stokes problems. Here and further N_{iter} is the *total* number of coupled preconditioned BiCGstab iterations for (25) performed solving a linear or nonlinear problem. A fixed number (eight) of multigrid V-cycles were performed to evaluate $\hat{A}^{-1}$ on each iteration of the BiCGstab. The linearized problem was solved in both forms: While the approximation results were almost the same and thus reflected only for rotation form, convergence of the solvers differ. In brackets [ ] we put numbers for convection form. Two factors have an impact on the convergence of iterations. The first one is the quality of preconditioner $\hat{A}$. As explained in Section 3 it becomes worse as $\nu/\gamma \to 0$. Another is a poor preconditioning of Schur complement as $\gamma \to 0$

Table 1
The effect of ∇div-stabilization for the linearized Navier–Stokes problem. Problem I ($h = 1/16$)

Viscosity		Value of γ				
		0	0.05	0.2	0.5	1.0
1e−1	$\|u - u_h\|$	1.9e−2	1.3e−2	8.6e−3	9.0e−3	1.3e−2
	$\|p - p_h\|$	4.3e−2	4.4e−2	4.9e−2	6.7e−2	1.3e−1
	$\|[e_h, q_h]\|$	4.1e−1	2.9e−1	1.8e−1	1.5e−1	1.8e−1
	N_{iter}	11 [11]	9 [10]	6 [8]	6 [5]	4 [4]
	ψ_{cd}	0.06 [0.07]	0.07 [0.08]	0.11 [0.19]	0.16 [0.32]	0.21 [0.39]
1e−3	$\|u - u_h\|$	1.8e−0	1.1e−1	8.0e−2	1.2e−1	1.4e−1
	$\|p - p_h\|$	3.3e−1	5.0e−2	4.6e−2	5.3e−2	6.0e−2
	$\|[e_h, q_h]\|$	3.1e−0	1.5e−1	9.0e−2	1.1e−1	1.2e−1
	N_{iter}	29[a] [div]	11 [12]	10 [16]	19 [33]	30 [92]
	ψ_{cd}	0.08	0.37 [0.64]	0.50 [0.77]	0.59 [0.85]	0.61 [0.89]

[a] Converges with modified pressure preconditioner only, ψ_{cd}—convergence factor in the MG-preconditioner for velocity problem.

and $\nu \ll 1$. For the rotation form setting $\hat{S}^{-1} = \nu\hat{M}^{-1} + \hat{S}_0^{-1}(\bar{\alpha})$ with auxiliary $\bar{\alpha} = 1$ cures the situation of $\gamma = 0$ and $\nu \ll 1$.

The best choice of γ is apparently $\gamma \approxeq 0.2$. We will use this value in our further experiments. The estimates (16) and (17) are in excellent agreement with the results from Table 1. We see that $|[\cdot]|$-norm is controlled independently of ν only for $\gamma > 0$. As predicted by (10), velocity, but not pressure, is sensitive to this stabilization. Although we present results only for $h = 1/16$, the situation is qualitatively the same, including the same value of optimal γ, for other values of mesh size.

Setting $\gamma = 0.2$ we test the solver for the linearized Problem I (rotation form). First we try the BiCGstab iterations for (25) with the inner velocity problem being solved almost exactly (up to 10^{-4} relative accuracy). The results (see Table 2) show the very robust behavior of the outer iterations to solve linearized Navier–Stokes problem (22) with respect to the mesh-size and viscosity (see discussion in Section 3). N_{outer} shows the number of outer coupled iterations needed for 10^{-6} reduction of the residual. At the same time the convergence of inner solver deteriorates as $\nu \to 0$, in fact as $\nu/\gamma \to 0$, resulting in a larger number of inner iterations for evaluation of $\hat{A}^{-1}$. The value of N_{inner} shows the average number of inner multigrid V-cycles with two pre- and post-smoothings needed *each* time to solve velocity problem. The number of inner iterations grows approximately as $O(\nu^{-1/2})$, reflecting the growth of the condition number for A. The dependence on h is caused by a poor smoothing property of smoothing iterations in the multigrid for small ν/γ.

The results from Table 2 are of *theoretical* interest, since solving the original nonlinear problem we neither solve the linearized one with high accuracy, nor we solve the inner velocity problem exactly, but perform only a fixed number of multigrid iterations (e.g., 2). Of course, the latter has a consequence that outer iterations become less robust, but a total computational work needed to achieve the same accuracy becomes much less.

Next we test a solver for the nonlinear problem. It was found that fixed point iterations known to be quite robust for two-dimensional the Navier–Stokes equations in convection form fail to be robust for rotation form, when viscosity is small. Therefore, for low ν we have to use implicit time stepping method with time step δt to obtain steady solutions. The time step depends on ν. In Table 3 we illustrate this effect solving problem I. We check the accuracy and the performance of the solvers. On each "time step" we perform four nonlinear iterations (21) and the stopping criteria in coupled BiCGstab iterations for linearized problem was the 0.1 reduction in the residual. To force the inner iterations to converge, we take δt small enough.

Further we present results for the driven cavity problem, see Tables 4, 5 and Fig. 3. We are interested in the results for this problem (at least) for the following reasons: Compared to problem I the solution is now *Re*-dependent and has boundary layers. The solution to the problem (velocity, pressure, and vorticity(!)) is singular in upper corners. In particular $\max_{\mathbf{x}} |\mathrm{curl}\, \mathbf{u}_h(\mathbf{x})| \to \infty$ as $h \to 0$. We note that no mesh adaptation was made.

Table 2
Convergence data of the BiCGstab for (25) with an exact velocity solver

$h = 1/32$				
Viscosity	2e−2	5e−3	1e−3	1e−4
N_{outer}	5	5	6	6
N_{inner}	13	27	65	230
$\nu = 1\text{e}{-3}$				
Mesh size	1/16	1/32	1/64	1/128
N_{outer}	5	6	6	6
N_{inner}	55	65	85	93

Table 3
Error in pressure and velocity, convergence data for nonlinear problem I in rotation form

Parameters		Mesh size			
		1/16	1/32	1/64	1/128
$\nu = 2e{-2}$	$\|u - u_h\|$	1.8e−2	5.3e−3	1.4e−3	3.5e−4
$\delta t = 1$	$\|p - p_h\|$	4.3e−2	1.5e−2	6.3e−3	3.0e−3
	N_{stp}	7	7	7	7
	N_{iter}	45	50	50	52
$\nu = 5e{-3}$	$\|u - u_h\|$	4.4e−2	1.4e−2	4.1e−3	1.2e−3
$\delta t = 0.25$	$\|p - p_h\|$	4.5e−2	1.5e−2	6.0e−3	2.8e−3
	N_{stp}	73	78	81	83
	N_{iter}	290	383	467	490

N_{stp}—number of time steps in BE method, N_{iter}—total number of iterations in linear solver.

Table 4
Convergence data, driven cavity problem

Reynolds number, method parameter γ		Mesh size			
		1/16	1/32	1/64	1/128
Rotation form					
	δt	1	0.25	0.166	0.1
$Re = 400$	N_{stp}	18	87	148	246
BE	N_{iter}	178	504	633	791
$\gamma = 0.2$	ψ_C	0.19	0.11	0.12	0.07
	δt	1	0.25	0.1	0.0625
$Re = 1000$	N_{stp}	30	67	151	279
BE	N_{iter}	183	381	582	1290
$\gamma = 0.2$	ψ_C	0.26	0.18	0.15	0.10
Convection form					
$Re = 1000$	N_{stp}	12	13	13	13
Fix-point	N_{iter}	301	581	903	1339
$\gamma = 0$	ψ_C	0.88	0.92	0.93	0.95
$Re = 1000$	N_{stp}	11	15	15	14
Fix-point	N_{iter}	78	151	202	225
$\gamma = 0.2$	ψ_C	0.65	0.75	0.8	0.83

N_{stp}—number of time steps in BE method, N_{iter}—total number of iterations in linear solver, ψ_C—convergence factor in coupled linear solver.

Table 5
Position of the center of the primary vortex and corresponding value of the streamfunction $\phi(x, y)$, $Re = 400$, convection formulation

Properties	Value of γ				
	$h = 1/32$			$h = 1/128$	Ref. [21]
	0	0.2	1.0	0.2	
$\phi(x, y)$	−0.0896	−0.0974	−0.0857	−0.1102	−0.1139
x	0.578	0.562	0.594	0.559	0.555
y	0.625	0.609	0.625	0.607	0.606

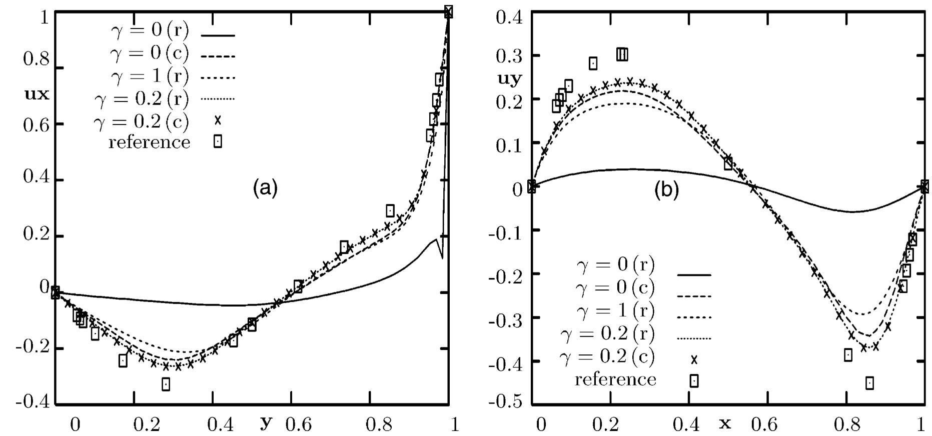

Fig. 2. (a) ux-component of velocity along the vertical center line of the cavity, $Re = 400$, $h = 1/32$; (b) uy-component of velocity along the horizontal center line of the cavity, $Re = 400$, $h = 1/32$; c—convection form, r—rotation form.

In Figs. 2 and 4 we compare the velocity profiles of the FE solutions with the reference data from ([21]) for $Re = 400$ and $Re = 1000$. For example, notation "1/16(r)" in the keys means that the corresponding solution was obtained on uniform grid with mesh-width 1/16 in pressure element and the rotation form of equations was used, and "$\gamma = 0.2$ (c)" means that convection form was used with parameter γ equals 0.2. We start with the case $Re = 400$ and study the effect of the ∇div terms. If ∇div-stabilization is used the results are the same for the schemes with different form of convection and are better then for non-stabilized or for schemes with values of parameter γ too far from optimal. From Fig. 2 one might conclude that ∇div-stabilization is a more crucial issue for the problem in rotation form. However this effect can be problem-dependent: Indeed, the kinematic pressure in the convection formulation has less impact to the error estimate (10 via the last trouble-making for $\gamma = 0$) term, compared to its counterpart in rotation formulation, Bernoulli pressure. Fig. 3, where isolines for both pressures are plotted, should give an impression

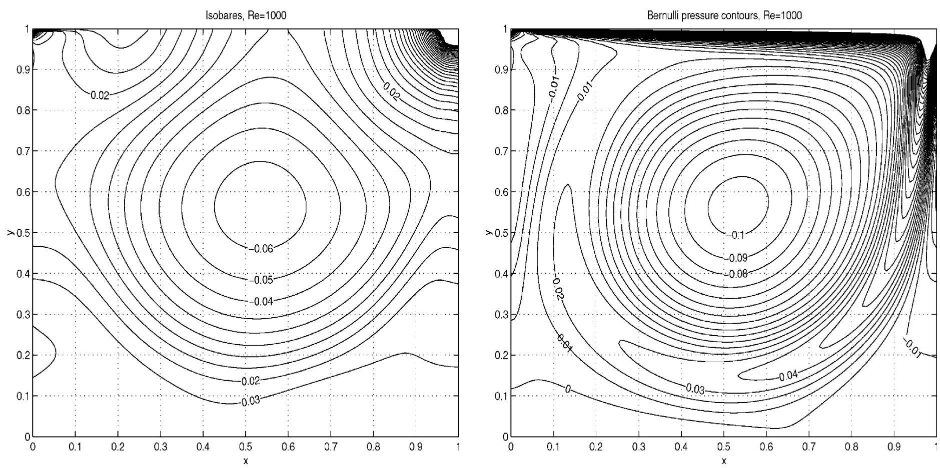

Fig. 3. Equidistantly distributed on interval $[-0.2, 0.3]$ isolines for kinematic pressure (left) and Bernoulli pressure (right) for the driven cavity with $Re = 1000$, $h = 1/128$.

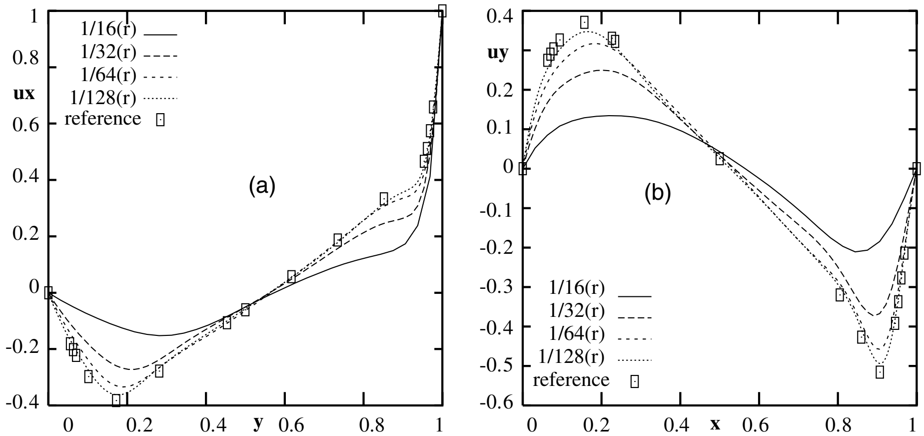

Fig. 4. Convergence of FE solution for the rotation formulation; (a) ux-component of velocity along the vertical center line of the cavity, $Re = 1000$; (b) uy-component of velocity along the horizontal center line of the cavity, $Re = 1000$.

that H^1 norm of the Bernoulli pressure is large than the same norm of the kinematic pressure for this particular problem. We can not claim that this is the case for an arbitrary flow, e.g. for analytical example I the norms of both pressures are comparable and the effect of $\gamma > 0$ is similar in both formulations.

Fig. 4 demonstrates stable convergence of the discrete solutions for the ∇div-stabilized rotation form with $\gamma = 0.2$.

The effect of choosing different values of γ is also illustrated in Table 5, where the position of a center and the minimal value of a streamfunction are given for the primary vortex of the calculated solutions with $Re = 400$. Results for the fine grid and from the Ref. [21] are given for comparison. The choice $\gamma = 0$, as well as $\gamma = 1$ ("overstabilized" problem), leads to less accurate values compared to $\gamma = 0.2$.

Figs. 5 and 6 show streamfunction isolines. For the easier comparison with results in [21] or [7] a selected (not equally distributed) streamfunction isolines are shown. The selection is the same as in [21]. For

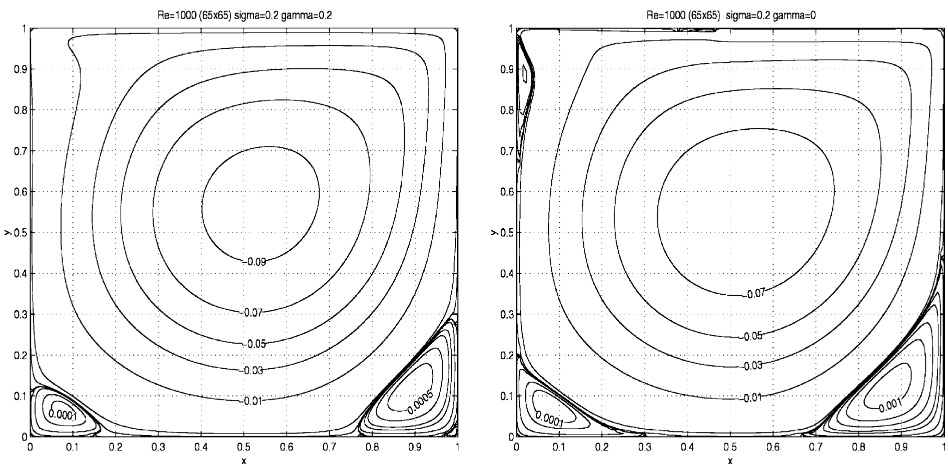

Fig. 5. Selected streamfunction isolines for the driven cavity with $Re = 1000$, $h = 1/32$. Convection form with the SUPG stabilization. ∇div-stabilized solution on the left figure and non-stabilized on the right.

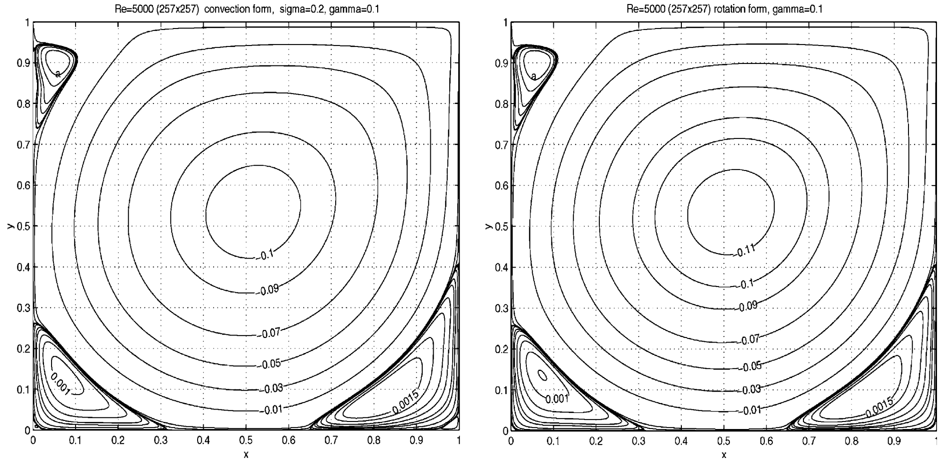

Fig. 6. Selected streamfunction isolines for the driven cavity with $Re = 5000$, $h = 1/256$. Solution for convection form with the SUPG and ∇div-stabilization on the left figure and for rotation form with the ∇div-stabilization on the right.

$Re = 1000$, comparing SUPG stabilized scheme with the usual Galerkin scheme for the convection formulation, we found that although the SUPG-stabilized solution is a bit more diffusive (less accurate) than non-stabilized one, the convergence of nonlinear iterations for the stabilized problem is considerably better (see also [44]). Moreover, to handle linearized equations in convection form the SUPG stabilization was also essential to ensure convergence of BiCGstab iterations for $Re \geqslant 1000$.

A proper value of γ remains to be important. Fig. 5 shows that a solution of the ∇div-stabilized scheme is more accurate for $h = 1/64$: On the right figure we see non-physical behaviour of the solution in the upper-left corner of the cavity, also the main vortex is approximated less accurately. For smaller h the difference becomes less visible, since both stabilized and non-stabilized schemes converge as $h \to 0$. Moreover the choice of $\gamma > 0$ reduces the total number of linear iterations (and hence the CPU time) dramatically (see Table 4), although a convergence in the internal multigrid method for the convection–diffusion problem becomes worse. The latter does not alter the total CPU time, since we perform a *fixed* number of multigrid cycles applying $\hat{A}^{-1}$ in (25).

Finally we compute a flow for $Re = 5000$. For high Reynolds numbers a flow becomes less steady and the linearized system poor conditioned. These result in a larger number of nonlinear iterations on the one hand and a worse convergence of inner linear iterations on the other hand. The former effect is more perceptible for the rotation form, the latter for the convection one. Partially these difficulties were overcome by using pseudo time stepping scheme: Time derivative $\partial\mathbf{u}/\partial t$ was replaced by $-\Delta\partial\mathbf{u}/\partial t$ (see, e.g., [26,32] for related technique) and $\delta t \in [100, 1000]$. Streamlines of solution are shown in Fig. 6, where the value of the label a for the left upper vortex equals 5×10^{-4}. The solution of the problem in convection form is a bit less accurate than the one of the problem in rotation form. The reason for the latter is that an additional diffusion via the SUPG terms was necessarily introduced in the first case. The corresponding total number of linear iterations needed for convergence (nonlinear residual $\leqslant 10^{-7}$) are 904 and 2670, respectively.

We make computations for the backward step problem using convection form of equations. For rotation form the ''do nothing'' outflow boundary conditions have poor performance for channel type flows. The reason is that the corresponding strong formulation of the boundary conditions is not satisfied by the Poisseuille flow, see also discussion in [29]. Streamfunction and kinematic pressure isolines for $Re = 800$ are plotted in Fig. 7. Table 6 compares calculated quantities with other experimental and numerical results found in literature. We note that in an experiment a flow is three-dimensional, so the difference with a

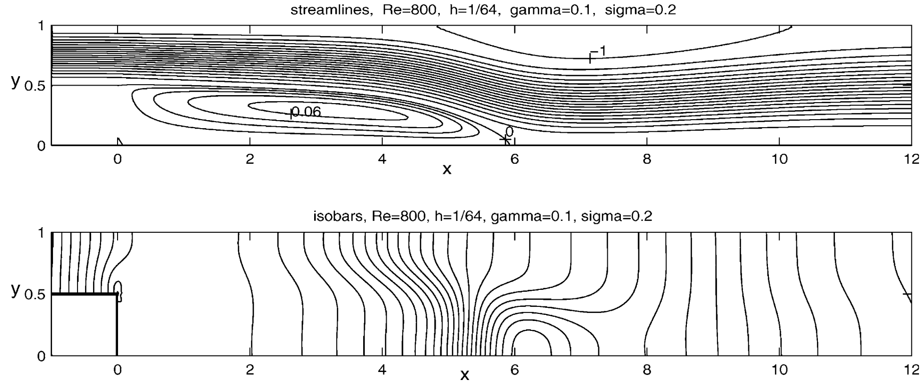

Fig. 7. Backward facing step problem for $Re = 800$, $h = 1/64$: selected streamlines and equally distributed on $[-1, 0]$ isobars for convection form with the SUPG and ∇div-stabilization.

Table 6
Numerical and experimental results the backward facing step problem

Configuration	Method	(x_c, y_c)	r_1	r_2	r_3	N_{iter}
$Re = 150$						
$\gamma = 0.1$, $\sigma = 0.2$	FE	(0.72, 0.29)	2.00	–	–	126
$\gamma = 0.1$, $\sigma = 0.0$	FE	(0.72, 0.29)	2.00	–	–	311
$\gamma = 0.0$, $\sigma = 0.2$	FE	(0.72, 0.29)	2.00	–	–	4044
Ref. [35]	Experimental	(0.91, 0.29)	2.25			
$Re = 800$						
$\gamma = 0.1$, $\sigma = 0.2$	FE	(3.31, 0.29)	5.88	4.85	10.13	1235
$\gamma = 0.0$, $\sigma = 0.2$	FE	(3.25, 0.29)	5.58	4.47	10.17	4180*
$\gamma = 0.1$, $\sigma = 0.2$	FE (1/64)	(3.32, 0.30)	5.94	4.85	10.21	1392
Ref. [19]	FD	(3.35, 0.30)	6.10	4.85	10.48	
Ref. [12]	Spectral		5.97	4.89	10.46	
Ref. [3]	Experimental		7.10			

(x_c, y_c)—position of the bottom vortex center, r_1—reattachment length for the bottom vortex, r_2—left separation point for the upper vortex, r_3—right reattachment point for the upper vortex, N_{iter}—total number of inner linear iterations in the fix-point method, $*$—total number of inner linear iterations in the pseudo time stepping scheme.

calculated two-dimensional solution should be expected. This difference becomes larger as Reynolds number grows. Notation "FE" stands for the finite element method from this paper with $h = 1/32$ (FE(1/64) denotes two times finer grid).

For $Re = 150$ numerical experiments with or without SUPG and ∇div-stabilization show the same values for low vortex center position and reattachment point. These values remain the same for solution calculated on a finer grid. However the total number of linear iterations in the fix-point method differs significantly, depending on particular stabilization used. When $\gamma = 0$ and $\sigma = 0$ iterations for the Oseen (linearized Navier–Stokes) problem fail to converge. For $Re = 800$ the SUPG stabilization is necessary to force the inner convection–diffusion solver to converge. The ∇div-stabilized method produced more accurate values of low vortex center position and seperation/reattachment points. Moreover, this stabilization is vital for convergence of the inner linear iterations for the Oseen problem. For $\gamma = 0$ we have to use pseudo time stepping scheme as described for the cavity problem with $Re = 5000$.

5. Conclusions

We outline the most important conclusions:

- The rotation form of the incompressible Navier–Stokes equations is a reasonable starting point for FE method and has the following *advantages*: Less computational work is required to calculate nonlinear terms; Effective solvers for the linearized problem are available, moreover SUPG-like stabilization was not found to be necessary for ensuring linear solvers convergence in the case of moderate or even high *Re* numbers; and *disadvantage*: Nonlinear iterations compared to the case of convection form are less robust. A reason and a possible cure of this disadvantage is the topic of current research.

Although for moderate Reynolds numbers the convection form has shown better CPU time than the rotation one in most tests with the *nonlinear* problem, we expect the situation can change for unsteady problems, when one is interested in evolutionary solutions. Moreover, due to the relatively simple structure of solvers for rotation form (block Jacobi smoothers and V-cycles) we see strong potential for parallel computations in this case.

- The ∇div stabilization enhances the accuracy of a solution and significantly improves the convergence of preconditioned iterations for the linearized Navier–Stokes problem. However the corresponding stabilization parameter should not be too large. If implicit scheme is used, more efficient multigrid methods for the anisotropic case $\nu/\gamma \ll 1$ are still desirable. For convection form the SUPG like stabilization improves the solvers performance, however it produces acceptable solutions (not too diffusive) for carefully and adaptively chosen stabilization parameters only.
- At the present moment, nonlinear iterations for the steady Navier–Stokes equations, e.g. of fix-point or quasi-Newton type, enhanced by the coupled preconditioned solvers for a linearized problem do not provide a robust engine for treating some, even relatively simple, flow problems. We see the bottleneck in missing a robust preconditioner for the Schur complement of the linearized problem in convection formulation or robust nonlinear iterations for the rotation formulation. At the same time the coupled methods remain the only feasible tool for treating steady problems, while so called projection or pressure-correction methods [39], based on decoupling velocity and pressure, were designed for treating unsteady problem and require too many time steps to converge to a steady state.

Acknowledgements

The author gratefully acknowledges many helpful discussions with G. Lube and A. Reusken. He also thanks A. Reusken, Yu. Vassilevskii, A.Wathen and unknown referees for the careful reading of the first version of the paper and many useful comments. Part of this work was done while the author was a visiting researcher at RWTH University in Aachen. Partially the work was supported by the Russian Foundation for Basic Research: grants No. 01-01-06310 linked to project 99-01-00263 and No 02-01-0615 linked to project 02-01-00592.

References

[1] M. Ainsworth, P. Coggins, The stability of mixed *hp*-finite element methods for Stokes flow on high aspect ratio elements, SIAM J. Num. Anal. 38 (2000) 1721–1761.
[2] T. Apel, G. Lube, Anisotropic mesh refinement in stabilised Galerkin method, Numer. Math. 74 (1996) 261–282.
[3] B.F. Armaly, F. Durst, J.C. Pereira, B. Schonung, Experimental and theoretical investigation of backward-facing step, J. Fluid. Mech. 127 (1983) 473–496.
[4] K. Arrow, L. Hurwicz, H. Uzawa, Studies in Nonlinear Programming, Standford University, Standford, 1958.

[5] P. Bastian, W. Hackbush, G. Wittum, Additive and multiplicative multigrid—A comparison, Computing 60 (1998) 345–364.

[6] S. Berrone, Adaptive discretization of the Navier Stokes equations by stabilized finite element methods, Comput. Methods Appl. Mech. Engrg. 190 (2001) 4435–4455.

[7] O. Botella, R. Peyret, Benchmark spectral results the lid-driven cavity flow, Comput. Fluids 4 (1998) 421–433.

[8] J. Bramble, J.E. Pasciak, A.T. Vassilev, Uzawa type algorithms for nonsymmetric saddle-point problems, Math. Comput. 69 (2000) 667–689.

[9] A.N. Brooks, T.J.R. Hughes, Streamline upwind/ Petrov-Galerkin formulation for convection dominated flows with particular emphasis on the incompressible Navier–Stokes equation, Comput. Methods Appl. Mech. Engrg. 32 (1982) 199–259.

[10] Ch.H. Bruneau, P. FabrieEffective, downstream boundary conditions for incompressible Navier–Stokes equations, Int. J. Numer. Meth. Fluids 19 (1994) 693–705.

[11] E.V. Chizhonkov, M.A. Olshanskii, On the domain geometry dependence of the LBB condition, Math. Model. Anal. Numer. (M2AN) 34 (2000) 935–951.

[12] C. Canuto, A. Russo, V. van Kemenade, Stabilized spectral methods for the Navier–Stokes equations: residual-free bubbles and preconditioning, Comput. Methods Appl. Mech. Engrg. 166 (1998) 65–83.

[13] R. Codina, Stabilization of incompressibility and convection through orthogonal sub-scales in finite element methods, Comput. Meth. Appl. Mech. Engrg. 190 (2000) 1579–1599.

[14] H.C. Elman, Multigrid and Krylov subspace methods for the discrete Stokes equations, Int. J. Numer. Meth. Fluids 22 (1996) 755–770.

[15] H.C. Elman, Preconditioning of the steady-state Navier–Stokes equations with low viscosity, SIAM J. Sci. Comp. 20 (1999) 1299–1316.

[16] H.C. Elman, D. Silvester, Fast nonsymmetric iterations and preconditioning for Navier–Stokes equations, SIAM J. Sci. Comp. 17 (1996) 33–46.

[17] L.P. Franca, S.L. Frey, Stabilized finite element methods: II. The incompressible Navier–Stokes equations, Comput. Methods Appl. Mech. Engrg. 99 (1992) 209–233.

[18] B. Fischer, A. Ramage, D. Silvester, A. Wathen, On parameter choice and iterative convergence for stabilised discretisations of advection–diffusion problems, Comput. Meth. Appl. Mech. Engrg. 179 (1999) 179–195.

[19] D.K. Gartling, A test problem for outflow boundary conditions–flow over the back-facing step, Int. J. Numer. Meth. Fluids 11 (1990) 953–967.

[20] V. Girault, P.A. Raviart, Finite Element Methods for Navier–Stokes Equations, Springer, Berlin, 1986.

[21] U. Ghia, K.N. Ghia, C.T. Shin, High-Re solutions for incompressible flow using the Navier–Stokes equations and a multigrid method, J. Comput. Phys. 48 (1982) 387–411.

[22] P.M. Gresho, Incompressible fluid dynamics: some fundamental formulation issues, Ann. Rev. Fluid Mech. 23 (1991) 413–453.

[23] P.M. Gresho, D.K. Gartling, J. Torezynski, K.A. Cliffe, K.H. Winters, T.J. Garrat, A. Spence, J.W. Goodrich, Is the steady viscous incompressible two-dimensional flow over a backward facing step at $Re = 800$ stable?, Int. J. Numer. Meth. Fluids 17 (1993) 501–541.

[24] M. Gunzburger, Finite Element Methods for Viscous Incompressible Flows. A Guide to the Theory, Practice and Algorithms, Academic Press, London, 1989.

[25] V. John, L. Tobiska, Numerical performance of smoothers in coupled multigrid methods for the parallel solution of the incompressible Navier–Stokes equations, Int. J. Numer. Meth. Fluids 33 (2000) 453–473.

[26] A. Jameson, W. Schmidt, E. Turkel, Numerical solution of the Euler equations by finite volume methods using Runge–Kutta time stepping schemes, AIAA Paper 81-1259, 1981.

[27] R.F. Hanby, D.J. Silvester, J.W. Chew, A comparison of coupled and segregate solution techniques for incompressible swirling flow, Int. J. Numer. Meth. Fluids 22 (1996) 353–373.

[28] S.K. Hannani, M. Stanislas, P. Dupont, Incompressible Navier–Stokes computations with SUPG and GLS formulations-A comparison study, Comput. Methods Appl. Mech. Engrg. 124 (1995) 153–170.

[29] J.G. Heywood, R. Rannacher, S. Turek, Artificial boundaries and flux and pressure conditions for the incompressible Navier–Stokes equations, Int. J. Numer. Meth. Fluids 22 (1996) 325–352.

[30] A. Klawonn, G. Starke, Block triangular preconditioners for nonsymmetric saddle point problem, Numer. Math. 81 (1999) 577–594.

[31] D. Kay, D. Loghin, A Green's function preconditioner for the steady state Navier–Stokes equations, Oxford University Computing Lab., Report 99/06, 1999.

[32] G.M. Kobelkov, On numerical methods of solving the Navier–Stokes equations in "velocity-pressure" variables, in: G.I. Marchuk (Ed.), Numerical Methods and Applications, CRC, New York, 1994, pp. 85–115.

[33] G. Lube, Stabilized Galerkin finite element methods for convection dominated and incompressible flow problems, Numer. Anal. Math. Model. (Banach center publications) 29 (1994) 85–104.

[34] G. Lube, M.A. Olshanskii, Stable finite element calculation of incompressible flow using the rotational form of convection, IMA J. Numer. Anal. 22 (2002) 437–461.

[35] K. Morgan, J. Periaux, F. Thomasset, Notes on Numerical Fluid Mechanics: Analysis of Laminar Flow Over a Backward Facing Step, vol. 9, Friedr. Vieweg, Braunschweig/Wiesbaden, 1984.
[36] S. Norburn, D. Silvester, Stabilized vs. stable mixed methods for incompressible flow, Comput. Methods Appl. Mech. Engrg. 166 (1998) 131–141.
[37] M.A. Olshanskii, An iterative solver for the Oseen problem and the numerical solution of incompressible Navier–Stokes equations, Numer. Linear Alg. Appl. 6 (1999) 353–378.
[38] M.A. Olshanskii, A. Reusken, Navier–Stokes equations in rotation form: A robust multigrid solver for the velocity problem, SIAM J. Sci. Comput. 23 (2002) 1683–1706.
[39] A. Prohl, Projection and Quasi-compressibility Methods for Solving the Incompressible Navier–Stokes Equations, B.G. Teubner, Stuttgart, 1997.
[40] A. Ramage, A multigrid preconditioner for stabilised discretisation of advection–diffusion problem, J. Comput. Appl. Math. 110 (1999) 187–203.
[41] R. Rannacher, Adaptive Galerkin finite element methods for partial differential equations, J. Comput. Appl. Math. 128 (2001) 205–233.
[42] M. Schafer, S. Turek, Benchmark computations of laminar flow around cylinder, in: E.H. Hirschel (Ed.), Flow Simulations with High-Performance Computers II Notes Numer. Fluid Mech. Vol. 2, 1996, pp. 547–566.
[43] D. Silvester, H.C. Elman, D. Kay, A. Wathen, Efficient reconditioning of the linearized Navier–Stokes equations, J. Comput. Appl. Math. 128 (2001) 261–279.
[44] S. Turek, Efficient Solvers for Incompressible Flow Problems: An Algorithmic Approach in View of Computational Aspects, LNCSE V.6, Springer, Berlin, 1999.
[45] S.P. Vanka, Block-implicit multigrid solutions of Navier–Stokes equations in primitive variables, J. Comput. Phys. 65 (1985) 138–158.
[46] R. Verfurth, L. Tobishka,Analysis, of a streamline diffusion finite element method for the Stoke and Navier–Stokes equations, SIAM J. Numer. Anal. 33 (1996) 107–127.
[47] H.A. van der Vorst, Bi-CGSTAB A fast and smoothly convergering variant of Bi-CG for the solution of nonsymmetric linear systems, SIAM J. Sci. Statist. Comut. 13 (1992) 613–644.
[48] A. Wathen, B. Fischer, D. Silvester, The convergence rate of the minimal residual method for the Stokes problem, Numer. Math. 71 (1995) 121–134.
[49] A. Wathen, personal communications.
[50] P. Wesseling, C.W. Oosterlee, Geometric multigrid with applications to computational fluid dynamics, J. Comput. Appl. Math. 128 (2001) 331–334.
[51] G. Wittum, Multigrid methods for Stokes and Navier–Stokes equations. Transforming smoothers-algorithms and numerical results, Numer. Math. 54 (1989) 543–563.
[52] L.B. Zhang, A second order upwinding finite difference scheme for the steady Navier–Stokes equations in primitive variables in a driven cavity with a multigrid solver, Math. Model. Anal. Numer. (M2AN) 24 (1990) 133–150.